Unexpected activation of carbon–bromide bond promoted by palladium nanoparticles in Suzuki C–C couplings†

Delphine Sanhes,[a] Eva Raluy,[a] Stéphane Rétory,[a] Nathalie Saffon,[b] Emmanuelle Teuma[a] and Montserrat Gómez*[a]

Received 24th March 2010, Accepted 2nd August 2010
DOI: 10.1039/c0dt00201a

Dihydroanthracene derivatives (**1–6**) containing imide (**1–3**) and amine (**4–6**) functions have been used for the stabilization of palladium nanoparticles, starting from Pd(0) and Pd(II) organometallic precursors. Well-dispersed nanoparticles of mean size in the range *ca.* 1.9 to 3.6 nm could be obtained using Pd(0) precursors (**PdLc** and **PdLd**, where **L** = **1–6** and **c** and **d** mean the organometallic precursor involved, [$Pd_2(dba)_3$] and [Pd(ma)(nbd)] respectively). With the aim to evaluate the behaviour of homogeneous species and nanoparticles used as catalytic precursors, palladium complex coordinated to the diamine **6**, [$Pd(OAc)_2(\kappa^2$-*N*,*N*-**6**)], was prepared, reporting for the first time the X-ray diffraction structure of a metallic complex containing a ligand with a 9,10-dihydroanthracene backbone. Palladium systems were evaluated in Suzuki C–C coupling reactions and relevant differences were observed comparing the reactivity of the homogeneous systems in relation to that obtained using palladium nanoparticles as starting catalyst in relation to the activation of the C–Br bonds for deactivated substrates.

Introduction

Palladium represents one of the most used catalysts in organic synthesis, mainly applied in versatile methods for the formation of C–C bonds, finding numerous industrial applications in fine chemicals production.[1] In the last decades, the synthesis of metal nanoparticles has become of great interest in the field of catalysis due to their size and high ratio of surface area to volume.[2] Under wet conditions, metallic nanoparticles become soluble heterogeneous catalytic species, showing the likely advantages of both homogeneous and heterogeneous classical catalysts.[3] Taking advantage of this multifaceted reactivity, we have recently proved the dual catalytic behaviour of palladium nanoparticles acting as reservoir of molecular species and also as heterogeneous catalyst (single-site and surface-like reactivity) by one sequential process involving two simple benchmark reactions, Heck C–C coupling followed by hydrogenation.[4]

In particular, the ligands involved in the stabilization of palladium nanoparticles play a crucial catalytic role in selective organic transformations.[5] For this reason, we are interested in the study of the coordination chemistry at the metallic surface. Actually, we provided evidence of a new mode of ligand coordination involving simultaneous π,π-interaction of the phenyl and pyridine fragments of 4-(3-phenylpropyl)-pyridine at the ruthenium nanoparticles surface.[6]

With these results in mind, we conceived ligands containing a 9,10-dihydroanthracene skeleton to be applied as palladium nanoparticles stabilizers (Scheme 1). Hydroanthracene derivatives have been employed in biochemistry (in anticancer chemotherapy,[7] as precursors of pyrrolines[8] and pharmacophores such as α,β-unsatured lactam or lactone compounds,[9] *etc*.) and also in catalysis (three-component Mannich reaction[10] or addition of diethylzinc to arylaldehydes[11]). However, to the best of our knowledge, this kind of ligands has not been previously reported as stabilizers of metallic nanoparticles.

Herein we report the synthesis and characterisation of new palladium nanoparticles coming from decomposition of different organometallic precursors in the presence of dicarboximides (**1–3**) and the corresponding heterocyclic amines (**4–6**) linked to a 9,10-dihydroanthracene backbone (Scheme 1). These nanocatalysts have been tested in C–C Suzuki cross-couplings between 4-substituted bromobenzene derivatives and phenyl boronic acid, showing the specific activation of aryl substrates by means of their interaction with the metallic surface, in contrast to the reactivity observed using molecular homogeneous systems.

Results and discussion

Synthesis of ligands

The condensation of 9,10-dihydroanthracene-9,10-α,β-succinic acid anhydride with the appropriate primary amine in toluene at reflux resulted in the formation of dicarboximides **1–3** in good yields (71–87%) (Scheme 1), based on the methodology previously reported by us.[12,13]

The heterocyclic amines **4–6** were obtained by reduction of the carbonyl groups with $LiAlH_4$ from the corresponding isolated

[a]*Laboratoire Hétérochimie Fondamentale et Appliquée UMR CNRS 5069, Université Paul Sabatier, 118 route de Narbonne, 31062, Toulouse cedex 9, France. E-mail: gomez@chimie.ups-tlse.fr.; Fax: +33 561558204; Tel: +33 561557738*
[b]*Université de Toulouse, UPS, Structure Fédérative Toulousaine en Chimie Moléculaire, FR2599, 118 route de Narbonne, 31062, Toulouse cedex 9, France*

† Electronic supplementary information (ESI) available: Calculated structures for complex **C6** (Fig. S1), TEM micrographs for **Pd1a**, **Pd2a**, **Pd4a**, **Pd5a**, **Pd1b**, **Pd2b**, **Pd4b**, **Pd5b**, **Pd1d**, **Pd3d**, **Pd4d** and **Pd6d** (Figs. S2, S3 and S4), X-ray powder diffraction data for **Pd2c**, **Pd6c**, **Pd2d** and **Pd5d** (Fig. S4) and IR data for PdNP and free ligands (Table S1). CCDC reference number 770513. For ESI and crystallographic data in CIF or other electronic format see DOI: 10.1039/c0dt00201a

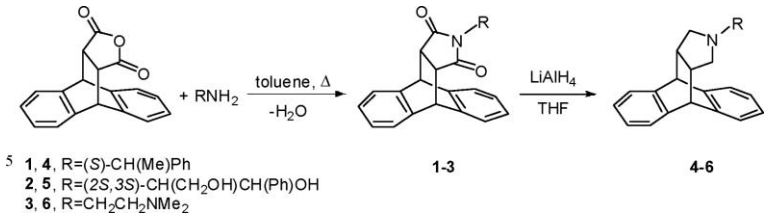

Scheme 1 Synthesis of dicarboximides **1–3** and amines **4–6**.

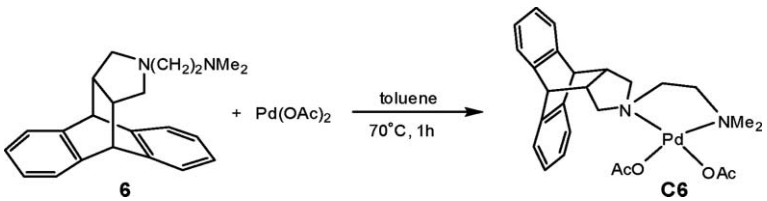

Scheme 2 Synthesis of [Pd(OAc)$_2$(κ^2-*N*,*N*′-**6**)], **C6**.

imides **1–3**, following the procedure described for **5** (Scheme 1).[13] Amines were obtained in quantitative yields.

Synthesis of [Pd(OAc)$_2$(κ^2-*N*,*N*-6)], C6

A coordination chemistry study was carried out with the diamine **6**. Reaction of Pd(OAc)$_2$ with 1 equivalent of **6** in toluene cleanly proceeded to give [Pd(OAc)$_2$(κ^2-*N*,*N*-**6**)] (**C6**) in 60% isolated yield (Scheme 2).

Yellow monocrystals were obtained from slow diffusion of diethyl ether on a solution of the complex in dichloromethane (Fig. 1). Even though crystal data have been reported concerning imides derived from 9,10-dihydroanthracene backbone,[14] **C6** represents the first coordination compound characterized in the literature by X-ray diffraction containing a ligand with this kind of skeleton.[15] The palladium atom is four-coordinated to two oxygen atoms of the acetate groups and two nitrogen atoms of ligand **6**, giving a five-membered metallacycle by bidentated coordination to the amine fragments. The coordination around the metal center is roughly square planar, with bond angles *ca.* 90°, except for the bite angle N1Pd1N2 (86°). The four bond lenghts around the metal center, Pd–O and Pd–N bonds, are quite similar (*ca.* 2.03 Å). The metallacycle adopts a distorted envelope conformation, where N1, N2, C4 and Pd1 atoms are quasi-coplanar (torsion angle C4–N2–N1–Pd1 = 12°) and the methylene carbon atom C3 is out of plane (torsion angle C3–C4–N1–Pd1 = 39°). The two five-membered cycles linked by the nitrogen atom N2 exhibit a quasi orthogonal spiro arrangement (torsion angle Pd1–C4–C22–C5 = 80°). The orientation of the metallacycle in relation to the 9,10-dihydroanthracene backbone places the Pd and acetate groups close to one of the aromatic groups; the opposite conformation with the methylene groups pointing to the aromatic fragment of the backbone was not observed. Modelling study for both conformers at DFT level (B3LYP, using 6-31G* polarization basis sets and pseudopotentials) showed a lower formation energy for the conformer observed by X-ray diffraction analysis (energy difference: +3.5 kcal mol^{-1}) (Fig. S1 in Supplementary information†).

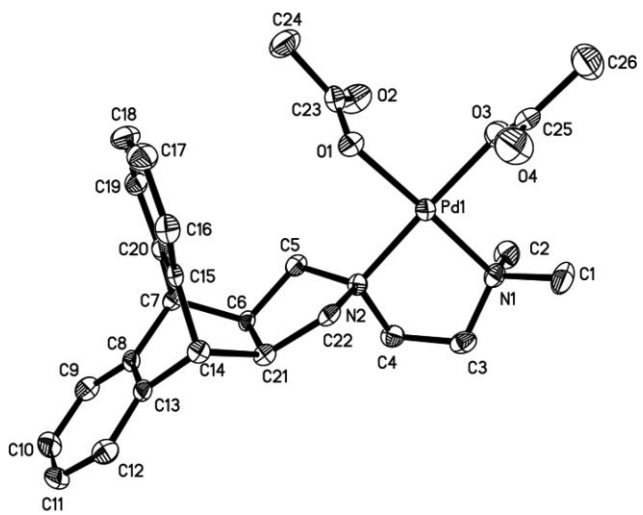

Fig. 1 View of the molecular structure of complex **C6**. Thermal ellipsoids are drawn at 50% probability level. Hydrogen atoms are omitted for clarity. Selected data: Pd1–N1 = 2.036(3); Pd1–N2 = 2.031(3) Å; Pd1–O1 = 2.034(2) Å; Pd1–O3 = 2.035(3) Å; N2–Pd1–O1 = 91.84(11); O1–Pd1–O3 = 91.03(10); N2–Pd1–N1 = 86.19(12); N1–Pd1–O3 = 90.99(11)°.

This complex was also characterized by elemental analysis, mass spectrometry, IR and NMR spectroscopies. Concerning the ^{1}H and ^{13}C NMR spectra, only one set of signals was observed. The protons corresponding to the two methylene groups located in the five-membered metallacycle are down-field shifted in relation to those corresponding to the free ligand (3.23 and 2.44 for complex **C6**, and 2.93 and 1.39 ppm for free ligand **6**). The two methyl groups bonded to the nitrogen atom are observed as two singlets in the ^{1}H NMR spectrum of the palladium complex (1.43 and 1.81 ppm), consistent with the bidentate coordination of the diamine **6**.

Synthesis of palladium nanoparticles

Both dicarboximides (**1–3**) and amines (**4–6**) were used as stabilizers of palladium nanoparticles (PdNP). Nanoparticles were prepared from decomposition of organometallic precursors under hydrogen atmosphere in order to reduce the metallic source and/or hydrogenate the ligands coordinated to the metal, in the presence of the appropriate stabilizer (**1–6**), based on the

methodology described by Chaudret's group (Scheme 3).[16] Palladium(II), $[PdCl_2(cod)]$ and $[Pd(\eta^3\text{-}C_3H_5)Cl]_2$, and palladium(0), $[Pd_2(dba)_3{\cdot}CHCl_3]$ and [Pd(ma)(nbd)], precursors were used in the synthesis of PdNP. The metallic nanoparticles were isolated by precipitation with pentane, giving black solids.

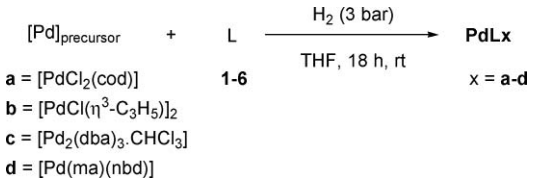

Scheme 3 Synthesis of PdNP stabilized by ligands **1–6** (cod = 1,5-cyclooctadiene; dba = dibenzylidenacetone; ma = maleic anhydride; nbd = norbornadiene).

Starting with palladium(II) organometallic precursors. $[PdCl_2(cod)]$ in the presence of **l**, **2**, **4** and **5** was treated with hydrogen in order to obtain the corresponding nanoparticles (**Pd1a**, **Pd2a**, **Pd4a** and **Pd5a**). Unfortunately, only agglomerates in the range of 5 to 100 nm could be observed in any case (Fig. S2 in Supplementary Information†). Their IR spectra (Table S1 in Supplementary Information†), recorded as KBr pellets in the range of 4000–400 cm^{-1}, exhibited the presence of the ligands in the composition of these materials. Comparing the main absorption bands of these PdNP to those of the corresponding free ligands, low shifts were observed, pointing to a weak interaction between the metallic surface and the ligand (Table S1, see Supplementary Information†). Similar results were obtained starting from $[Pd(\eta^3\text{-}C_3H_5)Cl]_2$ as organometallic precursor (**Pd1b**, **Pd2b**, **Pd4b** and **Pd5b**). Spherical agglomerates in the range of 10–200 nm were observed (Fig. S3 in Supplementary Information†).

These results indicate that Pd(II) precursors could not lead to the formation of well-defined nanoparticles, even for ligands **4** and **5** containing N-donor groups which should favour the coordination to the metallic surface.

Starting with palladium(0) organometallic precursors. $[Pd_2(dba)_3{\cdot}CHCl_3]$ in the presence of dicarboximides **1–3** (**Pd1c–Pd3c**) or amines **4–6** (**Pd4c–Pd6c**) under hydrogen conditions, led in all cases to the formation of palladium nanoparticles. The solutions coming from the work-up of these syntheses were analysed by ^1H NMR, showing the presence of dibenzylidenacetone (dba) and products corresponding to the partial reduction of dba. TEM micrographs corresponding to **Pd2c**, **Pd4c**, **Pd5c** and **Pd6c** showed the formation of small spherical nanoparticles with mean diameters in the range of 1.9 and 3.6 nm, depending on the ligand nature (Fig. 2).

The best dispersion of nanoparticles was observed for PdNP stabilized by the diamine **6**, **Pd6c** (Fig. 2e). **Pd1c** gave nanoparticles not homogeneous in size and **Pd3c** exhibited a sponge-like superstructure, pointing to aggregation of small individual particles.

[Pd(ma)(nbd)], containing labile and easily reducible ligands by hydrogenation, was also used as organometallic precursor for the synthesis of PdNP. This complex was prepared following the methodology described in the literature.[17] **Pd1d–Pd6d** were isolated by precipitation, washed with diethyl ether and dried under reduced pressure. The solutions coming from the work-up of these syntheses were analysed by ^1H NMR, showing the presence of maleic anhydride, succinic anhydride and norbornane. TEM micrographs for materials prepared in the presence of dicarboximides **1** and **3** or amines **4** and **6**, showed the formation of sponge-like superstructures constituted of aggregations of small individual particles (Fig. S4 in Supplementary Information†).

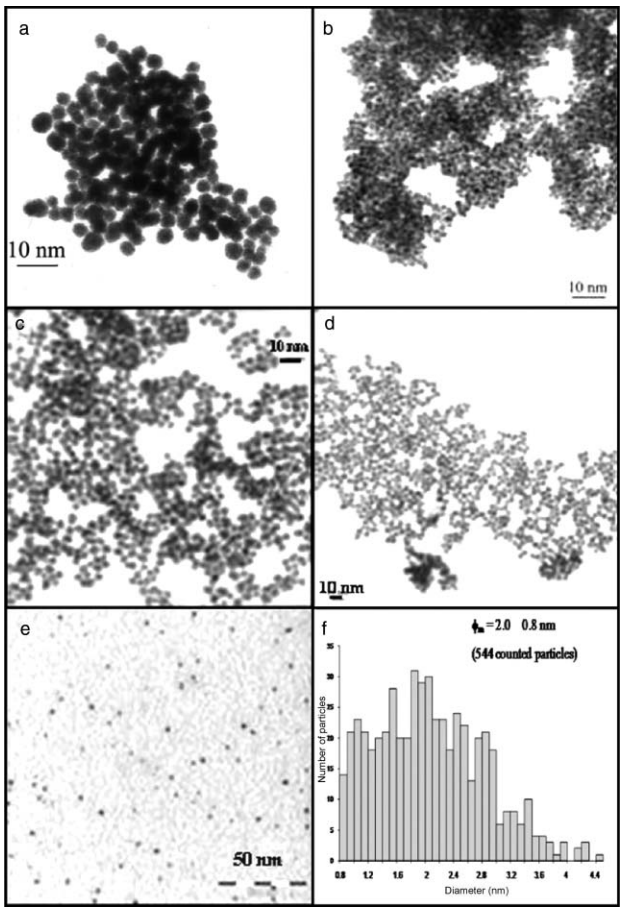

Fig. 2 TEM micrographs of PdNP from $[Pd_2(dba)_3{\cdot}CHCl_3]$ and dispersed in THF: a) **Pd1c**; b) **Pd2c** (1.9 ± 0.5 nm $[Pd_{247}]$); c) **Pd4c** (3.6 ± 1.2 nm $[Pd_{1678}]$); d) **Pd5c** (2.4 ± 0.9 nm $[Pd_{497}]$); e) **Pd6c** (2.0 ± 0.8 nm $[Pd_{288}]$) and f) size histogram for **Pd6c**. (In square brackets, the estimated cluster composition considering a compact packing of spherical nanoparticles showing a fcc arrangement).

In contrast, ligands **2** and **5** containing hydroxyl groups gave well-dispersed spherical nanoparticles, with mean diameters of 1.41 and 1.93 nm, respectively (Fig. 3). However, size distributions were relatively large. For these materials, Pd/ligand ratios of *ca.* 1/0.2 were found (from the elemental analyses) according to the synthesis conditions, but for **Pd3d**, **Pd4d** and **Pd6** a lower content in ligand ($Pd/L = 1/0.1$) was determined, in agreement with the big aggregates observed by TEM.

X-ray powder diffraction (XRD) of **Pd2c**, **Pd6c**, **Pd2d** and **Pd5d** showed the diffraction pattern corresponding to palladium showing a face-centered cubic packing (fcc) (Fig. S5 in Supplementary Information†).

To sum up, palladium nanoparticles of mean sizes *ca.* 2–4 nm could be obtained in the presence of imide and amine derivatives starting from palladium(0) organometallic precursors. The absence of any ligand leads to the formation of agglomerates.

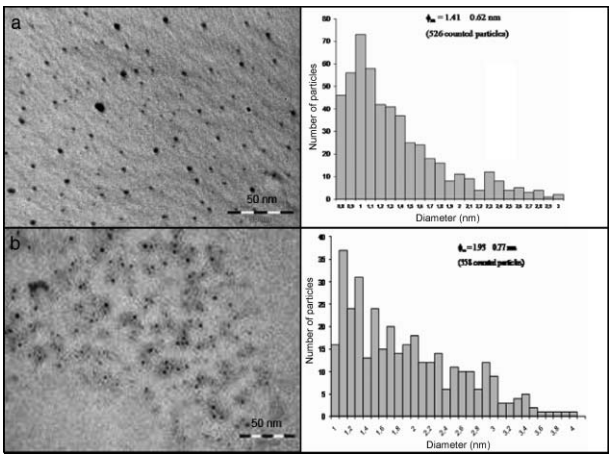

Fig. 3 TEM micrographs of PdNP from [Pd(ma)(nbd)] and dispersed in THF: a) **Pd2d** and b) **Pd5d** and their corresponding size histogram.

The presence of hydroxyl (**2** and **5**) and amine (**6**) moieties in the stabilizer favours the dispersion of nanoparticles. The differences in size observed for nanoparticles containing the same stabilizer (**2** or **5**) but prepared from different Pd(0) precursor, observing smaller particles when [Pd(ma)(nbd)] is involved (1.9 nm for **Pd2c** *vs.* 1.41 nm for **Pd2d** and 2.4 nm for **Pd5c** and *vs.* 1.95 nm for **Pd5d**), could be related to a faster nucleation process starting with [Pd(ma)(nbd)] than that with $[Pd_2(dba)_3{\cdot}CHCl_3]$, in agreement with the higher ability to be hydrogenated the coordinated ligands maleic anhydride and norbornadiene than that observed for dibenzylidenacetone under the same conditions (see above ^{1}H NMR analyses of work-up solutions). This fact could lead to an important concentration of nuclei in the case of [Pd(ma)(nbd)] and consequently favour the formation of smaller particles by the steric hindrance induced by the stabilizers around the nanoclusters.[18]

Catalytic results

Palladium nanoparticles obtained from decomposition of Pd(0) organometallic precursors were used as catalytic precursors for Suzuki C–C cross-coupling reactions, in particular those showing better dispersions containing ligands **2** and **5**: **Pd2c**, **Pd5c**, **Pd2d** and **Pd5d**. The catalytic reaction between bromobenzene substrates (R = OMe, CF_3) and phenyl boronic acid, was carried out under basic toluene–H_2O biphasic conditions (Scheme 4). The catalytic results are summarized in Table 1.

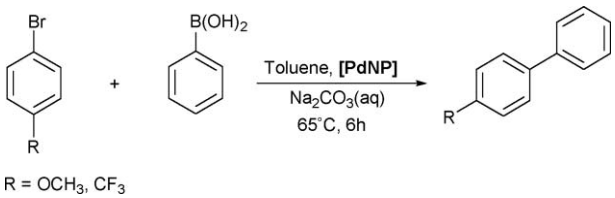

Scheme 4 Palladium nanoparticles catalyzed C–C cross-coupling between bromobenzene derivatives and phenyl boronic acid.

In all cases, the main product corresponded to the expected cross-coupling compound, with chemoselectivities higher than 92%. The best activities were achieved using PdNP resulting of [Pd(ma)(nbd)] decomposition in the presence of the dicarboximide **2**, **Pd2d** (entries 3 and 4, Table 1). Weaker activity was observed in the case of 4-bromoanisole than that related to 4-bromobenzotrifluoride due to the less activated carbon-bromide bond for the oxidative addition (entry 3 *vs.* 4, Table 1). **Pd2d** was also tested as catalytic precursor for the coupling between 4-chlorobenzotrifluoride and the phenyl boronic acid, but no activation of C–Cl bond was observed. On the other hand, **Pd2c** activated 4-bromobenzotrifluoride, but it was inefficient for the methoxy analogous substrate (entry 1 *vs.* 2, Table 1).

Table 1 Suzuki C–C cross-coupling of bromobenzene derivatives with phenyl boronic acid using PdNP as catalytic precursors (Scheme 4)[a]

Entry	Catalytic precursor	*R*	Conversion (%)[b]	Selectivity (%)[b]
1	**Pd2c**	OCH_3	0	—
2	**Pd2c**	CF_3	73	92[c]
3	**Pd2d**	OCH_3	81	95[c]
4	**Pd2d**	CF_3	100	100
5	**Pd5c**	OCH_3	50	100
6	**Pd5c**	CF_3	43	100
7	**Pd5d**	OCH_3	58	100
8	**Pd5d**	CF_3	62	92[c]

[a] Reaction conditions: Pd:aryl bromide:phenyl boronic acid:sodium carbonate = 1 : 100 : 150 : 200 mmol in 3 cm^3 of toluene and 1 cm^3 of water; all reactions in duplicate. [b] Arylbromide conversion and selectivity in cross-coupling product determined by GC. [c] Benzene was detected as the only by-product by GC.

According to the mechanism generally accepted for the Suzuki C–C cross-coupling catalyzed by molecular palladium species, better conversions are obtained using substrates containing electron-withdrawing groups than those containing electron-donor groups.[19,20] Thus, the results obtained using **Pd2c** and **Pd2d** as catalytic precursors, mainly for **Pd2c**, indicate that the reactivity of these nanoparticles is rather similar to that expected using molecular complexes. **Pd2c** and **Pd2d** seem to act as a reservoir of catalytically active molecular species released from the metallic surfaces.[21]

In contrast, the catalytic activity of **Pd5c** and **Pd5d** remained unchanged for both aryl bromide substrates used (entry 5 *vs.* 6 and entry 7 *vs.* 8, Table 1). These results indicate a higher activity for 4-bromoanisole than that expected on the basis of the molecular Pd-catalyzed mechanism. This activation enhancement for 4-bromoanisole could be due to the interaction of the methoxy group with the metallic surface inducing a higher activation of the C–Br bond than that expected only for intrinsical electronic reasons of the substrate.

The differences observed between nanoparticles containing ligands **2** and **5** can be related to a higher stability of PdNP when the heterocyclic amine **5** is used as stabilizer than that produced by the corresponding imide (ligand **2**), being faster the interaction of the substrate with the surface than the leaching of molecular species for PdNP stabilized by amine **5**. Therefore, for **Pd5c** and **Pd5d**, the methoxy substrate interacts with the metallic surface before the oxidative addition could take place, inducing a higher reactivity of the C–Br bond, similar to that observed for the trifluoromethyl-substituted aryl substrate for which the interaction with the metallic surface is not favoured.

In order to compare the surface-like and molecular reactivity, nanoparticles containing the diamine **6** (**Pd6c**) and the corresponding molecular complex **C6** (see above) were tested as catalytic precursors in the Suzuki C–C cross-coupling reactions (Scheme 4),

Table 2 Suzuki C–C cross-coupling of 4-R-bromobenzene derivatives with phenyl boronic acid using **Pd6c** nanoparticles and **C6** complex as catalytic precursors[a]

Entry	Catalytic precursor	*R*	Conversion (%)[b]
1	**C6**	CF_3	99[c]
2	**C6**	OPh	99
3	**C6**	SMe	83
4	**C6**	OMe	64[c]
5	**Pd6c**	CF_3	83
6	**Pd6c**[d]	OPh	5
7	**Pd6c**	SMe	66
8	**Pd6c**	OMe	99
9	**Pd6c+6**[e]	SMe	6
10	**Pd6c+6+KOAc**[f]	SMe	28

[a] Reaction conditions: Pd:aryl bromide:phenyl boronic acid:sodium carbonate = 1 : 100 : 150 : 200 mmol in 3 cm^3 of toluene and 1 cm^3 of water; all reactions in duplicate. [b] Arylbromide conversion and selectivity in cross-coupling product determined by GC. [c] Arylbromide conversion and selectivity in cross-coupling product determined by ^{1}H RMN. [d] Conversion = 5% after addition of 1 equivalent of ligand; conversion = 5% after addition of 2 equivalents of potassium acetate; conversion = 5% after addition of 1 and 2 equivalents of ligand and potassium acetate respectively. [e] Addition of 1 equivalent of ligand **6**. [f] Addition of 1 equivalent of ligand **6** and 2 equivalents of potassium acetate.

enlarging the number of substrates (4-R-bromobenzene derivatives: R = OMe, CF_3, OPh, SMe) in order to evidence the effect of the activation of the C–Br bond by the metallic surface.

Both catalytic systems gave an excellent chemoselectivity, yielding exclusively the corresponding cross-coupling product for bromobenzene derivatives where R = CF_3, OPh, SMe and OMe (entries 1–4 for molecular catalytic precursor **C6** and entries 5–8 for palladium nanoparticles catalytic precursor **Pd6c**, Table 2). For the molecular catalytic system **C6**, the best activities were obtained using 4-bromobenzotrifluoride and 4-bromodiphenylether (entries 1 and 2, Table 2), as expected for the substrates containing electron-withdrawing and poorly electron-donor groups; consequently, the molecular catalytic system was less active when 4-bromothioanisole and 4-bromoanisole were involved (entries 3 and 4, Table 2). However using **Pd6c** as catalytic precursor, for anisole (entry 8, Table 2), thioanisole (entry 7, Table 2) and diphenylether (entry 6, Table 2) bromobenzene substrates, the group showing a higher electron-donor ability (methoxy derivative) exhibited higher activity in relation to OPh and SMe moieties; in particular 4-bromodiphenylether (entry 6, Table 2) was practically inactive, probably due to the π,π-coordination of both aromatic rings at the metallic surface as previously observed using Ru nanoparticles.[6] For this catalytic reaction, the addition of extra ligand and/or the addition of acetate salt did not induce an activity increase of the system. Furthermore, addition of free ligand and potassium acetate in the catalytic reaction involving SMe-containing substrate triggered a decrease on the activity (entries 7, 9 and 10, Table 2), which means that the substrate is less available to the metallic surface and in consequence the activity decreases. Even under these catalytic conditions, the molecular leaching is not favoured (entry 3 *vs.* 10, Table 2).

These results corroborate the interaction of 4-R-bromobenzene at the metallic surface, both improving the reactivity of the C–Br bond for deactivated substrates such as 4-bromoanisole and inhibiting the cross-coupling by strong coordination on the surface such as in the case of 4-bromodiphenylether.

Conclusions

In summary, we could isolate palladium nanoparticles stabilized by new functionalized ligands with a 9,10-dihydroanthracene backbone (**1–6**) by decomposition of palladium(0) organometallic precursors. Heterocyclic amines **5** and **6** containing hydroxy and dimethylamino groups gave metallic nanoparticles stable under catalytic C–C Suzuki conditions. This fact favoured the interaction of the substrates with the metallic surface, inducing a higher activation of the C–Br bond for the 4-bromoanisole substrate than that produced for 4-bromobenzotrifluoride, on the contrary to the reactivity expected for molecular homogeneous systems. For this purpose, the complex [Pd(OAc)$_2$(κ^2-*N*,*N*′-**6**)] containing the diamine **6** was prepared and fully characterized. Actually, the homogeneous system favoured the coupling when 4-bromobenzotrifluoride was used as substrate. Therefore, the activation enhancement of the C–Br bond for 4-bromoanisole using PdNP as catalytic precursors is probably promoted by the interaction of the methoxy group with the metallic surface diminishing its electron-donor character, and in consequence favouring the oxidative addition of the C–Br bond with the metal. Furthermore, 4-bromodiphenylether did not lead to the formation of the cross-coupling product when PdNP were used as catalytic precursor in contrast to the high activity observed when the molecular complex was involved. These facts demonstrate that the substrate interacts with the metallic surface and the activation of C–Br bond is feasible depending on the substrate substituent; substrate coordination and steric effects can strongly tune the catalytic reactivity. A dramatic decrease on the activity was observed for 4-bromothioanisole when extra ligand and/or acetate salt were added, showing the stability of the PdNP in the reaction medium, protected by ligands and salts which avoid the approach of the substrate at the metallic surface. The nature of the catalytic species after substrate activation remains uncertain (Scheme 5).

Experimental

General

All operations were carried out using standard Schlenk or Fischer–Porter bottle techniques. The organic solvents were purified by standard procedures and distilled under argon atmosphere: toluene, diethyl ether and THF over sodium benzophenone and pentane over calcium hydride. Ligands **1**,[12] **2** and **5**,[13] and [Pd(ma)(nbd)][17] were obtained following the procedure previously described. NMR spectra were recorded on an Advance 500 Bruker spectrometer equipped with a CryoFlowProbe (^{1}H, standard $SiMe_4$) in CH_3OD. The ^{1}H NMR monitoring was performed in the NMR tube (Wilmad NMR tube w/J. Young valve, 5 mm). IR spectra were performed on a Perkin Elmer IR-FT 1760-X spectrophotometer at the "Service Commun d'Infrarouge de la Structure Fédérative de Toulouse" using KBr pellets after isolation of the particles as solids. Elemental analyses were carried out at the "Service central d'analyse du CNRS de Vernaison". TEM analyses were performed on a JEOL JEM 1011 transmission electron microscope running at 100 kV with a point resolution of 4.5 Å, at the "Service Commun de Microscopie Electronique de l'Université Paul Sabatier, TEMSCAN". A drop of colloidal

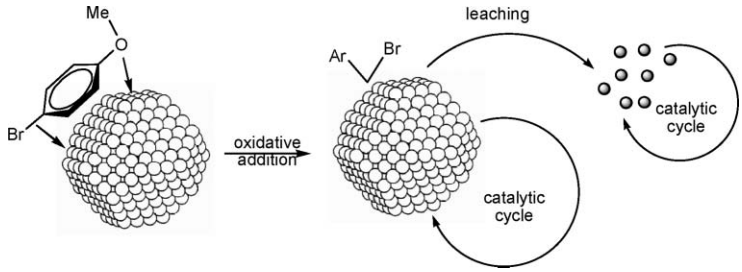

Scheme 5 Activation of 4-bromoanisole promoted by the metallic surface of palladium nanoparticles.

solution was deposited onto a holey carbon covered copper grid. The digital acquisition of the images was recorded by a camera height of column wide angle SIS (Megaview III). The size of the particles was determined by means of the software of treatment of images "Image-J". GC analyses were carried out on an Agilent GC6890 with a flame ionization detector, using a SGE BPX5 column composed by 5% of phenylmethylsiloxane. Powder X-ray diffraction measurements were performed at room temperature placing the samples in capillary tubes, on a Panalytical MPDPro diffractometer equipped with a multi-shell mirror working in transmission mode and with a fast linear X'Célérator detector; the analyses were carried out at the "Service de diffraction de rayons X du Laboratoire de Chimie de Coordination" in Toulouse. Modelling studies have been carried out using the following software: Spartan '06 for Windows and Linux. Wavefunction, Inc. 18401 Von Karman Avenue, suite 370. Irvine, CA 92612 USA.

Synthesis of ligands 9,10,11,15-tetrahydro-(11*S*,15*S*)-(*N*,*N*-dimethylethylenediamine)-9,10-pyrollanthracen-12,14-dione, 3

A solution of 9,10-dihydroanthracene-9,10-α,β-succinic acid anhydride (1.00 g, 3.6 mmol) and *N*,*N*-dimethylethylene-diamine (0.4 cm^3, 3.6 mmol) in toluene (50 cm^3) was refluxed for 72 h in the presence of molecular sieves 4 Å. The reaction mixture was then cooled, filtered and the solvent removed under reduced pressure. The residue obtained was dissolved in dichloromethane (20 cm^3) and washed with ammonium chloride saturated aqueous solution (3 × 20 cm^3). The combined organic layers were dried on anhydrous Na_2SO_4, filtered and the solvent was evaporated under vacuum leading to a white powder (0.97 g, 77%). Mp 203 °C; ν_{max}(KBr pellet)/cm^{-1} 3072, 3042, 3026 and 3012 (=CH), 2977, 2951, 2859 and 2815 (C–H), 1704 (CO), 1479 and 1465 (C=C), 1148 (C–N); δ_H(300 MHz; $CDCl_3$; 298 K) 1.66 (2H, t, *J* 6.0, $CH_2N(CH_3)_2$), 2.08 (6H, s, $2CH_3$), 3.13 (2H, t, *J* 6.0, $CH_2N(CO)_2$), 3.17 (2H, s, 2CHCON), 4.71 (2H, s, 2CH–Ph), 7.08 (4H, m, 2CH=CH), 7.21 (4H, m, 2CH=CH), 7.31 (4H, m, 2CH=CH); δ_C(75.5 MHz; $CDCl_3$; 298 K) 35.7 ($CH_2N(CH_3)_2$), 45.0 (2CH–Ph or 2CH-CON or $2CH_3$), 45.6 (2CH–Ph or 2CH-CON or $2CH_3$), 46.9 (2CH–Ph or 2CH-CON or $2CH_3$), 55.2 ($CH_2N(CO)_2$), 126.9–124.2 (Caromatic), 138.8 (Caromatic), 141.5 (Caromatic), 176.4 (CO), 176.8 (CO); *m*/*z* (EI) 346 ($M^{+\bullet}$ $C_{22}H_{22}N_2O_2^+$ requires 346.4).

9,10,11,15-tetrahydro-(11*S*,15*S*)-(*N*-(*S*)-methylbenzylamine)-9,10-pyrollanthracene, 4

Compound **1** (500 mg, 1.30 mmol) was dissolved in freshly distilled THF (25 cm^3) and the resulting suspension was vigorously stirred until total dissolution. The reaction mixture was then cooled at 0 °C and $LiAlH_4$ (750 mg, 20.0 mmol) was slowly added, giving a white suspension. The mixture was heated at reflux for 48 h. Diethylether (20 cm^3) and a saturated aqueous solution of Na_2SO_4 were then added at 0 °C. The addition of the aqueous solution was slowly performed and stopped when effervescence was no longer observed in the reaction mixture. The white product was then filtered over Celite and washed several times with a mixture of CH_2Cl_2–MeOH (9 : 1). The organic phase was washed with water (3 × 20 cm^3), dried with anhydrous Na_2SO_4, filtered and concentrated at reduced pressure, yielding the corresponding amine. Compound **4** was obtained as brown oil (0.46 g, 99%). mp 137 °C; (Found: C, 88.5; H, 7.1; N, 3.4. Calc. for $C_{26}H_{21}NO_2$: C, 88.9; H, 7.2; N, 3.9%); ν_{max}(KBr pellet)/cm^{-1} 3062 (=CH), 2927 (C–H), 1654 and 1457 (C=C); δ_H(300 MHz; $CDCl_3$; 298 K) 1.10 (3H, t, *J* 6.0, CH_3), 1.72 (2H, m, CH_2N), 2.58 (4H, m, CH_2N, 2CHCH$_2$N), 2.82 (1H, m, CHN), 4.01 (1H, d, *J* 3.0, CH–Ph), 4.06 (1H, d, *J* 3.0, CH–Ph), 7.05 (13H, m, CH=CH); δ_C(100.6 MHz; $CDCl_3$; 298 K) 22.8 (CH_3), 44.1 (CHCH$_2$N), 44.2 (CHCH$_2$N), 47.7 (CH–Ph), 47.8 (CH–Ph), 56.0 (CH_2N), 56.1 (CH_2N), 65.6 (CHN), 123.5–128.1 (Caromatic), 142.0–144.2 (Caromatic); *m*/*z* (CI, NH_3) 352.2 (M + $H^{+\bullet}$ $C_{26}H_{21}NO_2^+$ requires 352.5).

9,10,11,15-tetrahydro-(11*S*,15*S*)-(*N*,*N*-dimethyl-ethylenediamine)-9,10-pyrollanthracene, 6

Compound **3** (200 mg, 0.58 mmol) was dissolved in freshly distilled THF (25 cm^3) and the resulting suspension was vigorously stirred until total dissolution. The reaction mixture was then cooled at 0 °C and $LiAlH_4$ (330 mg, 8.7 mmol) was slowly added, giving a white suspension. The mixture was heated at reflux for 24 h. Diethylether (20 cm^3) and a saturated aqueous solution of Na_2SO_4 were then added at 0 °C. The addition of the aqueous solution was slowly performed and stopped when effervescence was no longer observed in the reaction mixture. The white product was then filtered over Celite and washed several times with CH_2Cl_2. The organic phase was washed with a saturated aqueous solution of NaCl (3 × 20 cm^3), dried with anhydrous Na_2SO_4, filtered and concentrated at reduced pressure, yielding the corresponding amine. Compound **6** was obtained as a white powder (0.17 g, 91%). mp 145 °C; ν_{max}(KBr pellet)/cm^{-1} 3065, 3039 and 3017 (=CH), 2927, 2860, 2840, 2823, 2800 and 2774 (C–H), 1466 and 1456 (C=C), 1140 (C–N); δ_H(300 MHz; $CDCl_3$; 298 K) 1.40 (2H, t, *J* 6.0, $CH_2N(CH_3)_2$), 2.10 (6H, s, $2CH_3$), 2.23 (4H, m, 2CHCH_2N), 2.62 (2H, m, 2CHCH$_2$N), 2.93 (2H, t, *J* 6.0, CHNCH_2), 4.05 (2H, s, 2CH–Ph), 7.01 (4H, m, CH'CH), 7.17 (4H, m, CH=CH); δ_C(100.6 MHz; $CDCl_3$; 298 K)

44.4 ($CHCH_2N$), 45.8 (CH_3), 47.0 (CH–Ph), 54.4 ($CHCH_2N$), 57.5 ($CHNCH_2$, $CH_2N(CH_3)_2$), 58.0 ($CHCH_2N$), 123.7–125.9 (*C*Haromatic), 141.9–144.2 (*C*aromatic); *m/z* (CI, NH_3) 319.4 ($M + H^{+\bullet}$ $C_{22}H_{26}N_2^+$ requires 319.5).

Synthesis of [Pd(OAc)$_2$(κ^2-*N*,*N*-6)] complex, C6

Amine **6** (100 mg, 0.314 mmol) was dissolved in 15 cm^3 of toluene and $Pd(OAc)_2$ (63 mg, 0.284 mmol) was then added. This mixture was stirred for 1 h at 70 °C. The solvent was then evaporated to give a green solid. Recrystallization from dichloromethane:diethylether (1 : 5) at 4 °C afforded [Pd(OAc)$_2$(κ^2-*N*,*N*-**6**)] complex as yellow crystals (91 mg, 0.167 mmol, 60%).(Found: C, 56.1; H, 6.2; N, 4.8. Calc. for $C_{26}H_{32}N_2O_4Pd$: C, 57.5; H, 5.9; N, 5.1%); ν_{max}(KBr pellet)/cm^{-1} 2960–2851 (C–H), 1625–1590 (C═O), 1020 (C–O); δ_H(300 MHz; $CDCl_3$; 298 K) 1.43, 1.81 (6H, s, 2CH_3), 2.44, (2H, m, CH_2NCH$_3$), 2.47 (4H, s, 2CH_2N), 2.52 (6H, s, 2C*H*3CO), 2.67 (2H, m, 2C*H*CH$_2$N), 3.23 (2H, m, CH_2NCH$_2$), 4.06 (2H, s, 2C*H*–Ph), 7.20–7.00 (8H, m, C*H*═C*H*). δ_C(100.6 MHz; $CDCl_3$; 298 K) 22.8, 23.4 (2C, NCH_3), 42.1 (2C, *C*HCH$_2$N), 45.4 (2C, *C*HC═C), 50.7 (2C, *C*H$_3$–CO), 58.2 (1C, CH*C*H$_2$N), 60.1 (1C, N*C*H$_2$CH$_2$), 62.7 (1C, CH*C*H$_2$N), 64.4 (1C, *C*H$_2$NCH$_3$), 126.9–123.8 (8C, *C*H aromatic), 143.6–139.6 (4C, *C*aromatic), 178.1 (2C, *C*═O); *m/z* (CI, NH_3) 483 (M-OAc$^+$. $C_{24}H_{29}N_2O_2Pd$ requires 483.9).

General procedure for synthesis of Pd nanoparticles

From decomposition of [PdCl$_2$(cod)]. 0.35 mmol of palladium precursor [$PdCl_2$(cod)] (100 mg) and 0.2 equivalents of ligand (0.07 mmol; 26.5 mg for **1**; 30.0 mg for **2**; 12.2 mg for **4**; 13.9 mg for **5**) were dissolved in 80 cm^3 of dried and degassed THF, and the system was then pressurised with three bar of hydrogen in a Fischer–Porter bottle. In few minutes, the initially yellow solution became black. The reaction mixture was then stirred at room temperature for 18 h. The hydrogen was replaced by argon and the volatiles removed under reduced pressure. The black solid was dispersed in 2 cm^3 of THF and some drops were used for TEM analyses.

From decomposition of [Pd(η^3-C$_3$H$_5$)Cl]$_2$. 0.27 mmol of palladium precursor [Pd(η^3-C_3H_5)Cl]$_2$ (50 mg) and 0.2 equivalents of ligand (0.055 mmol; 20.7 mg for **1**; 23.2 mg for **2**; 19.2 mg for **4**; 21.7 mg for **5**) were dissolved in 80 cm^3 of dried and degassed THF, and the system was then pressurised with three bar of hydrogen in a Fischer–Porter bottle. In few minutes, the initially yellow solution became black. The reaction mixture was then stirred at room temperature for 18 h. The hydrogen was replaced by argon and the volatiles removed under reduced pressure. The black solid was dispersed in 2 cm^3 of THF and some drops were used for TEM analyses.

From decomposition of [Pd$_2$(dba)$_3$·CHCl$_3$]. 0.19 mmol of palladium precursor [Pd_2(dba)$_3$·$CHCl_3$] (100 mg) and 0.2 equivalents of ligand (0.039 mmol; 14.6 mg for **1**; 16.4 mg for **2**; 13.5 mg for **3**; 15.3 mg for **4**; 13.4 mg for **5**; 13.6 mg for **6**) were dissolved in 80 cm^3 of dried and degassed THF, and the system was then pressurised with three bar of hydrogen in a Fischer–Porter bottle. In few minutes, the initially yellow solution became black. The reaction mixture was then stirred at room temperature for 18 h. In few minutes, the initially red solution became black. The reaction mixture was then stirred at room temperature for 18 h. The hydrogen was replaced by argon and the volatiles removed under reduced pressure. The resulting black solid was further washed with pentane (3 × 5 cm^3), concentrated *in vacuum* and then dispersed in 2 cm^3 of THF for TEM analyses. The isolated particles were also analysed by IR spectroscopy and elemental analysis.

(**Pd2c**: Found: C, 40.5; H, 4.7; N, 1.6; Pd, 39.4. Calc. for Pd_5(**2**)$(THF)_{4.6}(H_2O)_{3.2}$: C, 40.5; H, 4.9; N, 1.1; Pd, 39.5%. idealized formula taking into account the size determined by TEM and considering a compact packing arrangement of spherical nanoparticles: [Pd_{247}(**2**)$_{49}(THF)_{227}(H_2O)_{158}$]; **Pd3c**: Found: C, 30.4; H, 3.2; N, 1.6; Pd, 45.4. Calc. for Pd_5(**3**)$_{0.7}(THF)_{3.9}(H_2O)_4$: C, 34.9; H, 4.9; N, 0.6; Pd, 45.8%.; **Pd4c**: Found: C, 24.1; H, 2.1; N, 1.6; Pd, 60.7. Calc. for Pd_5(**4**): C, 35.3; H, 2.8; N, 1.6; Pd, 60.2%; idealized formula taking into account the size determined by TEM and considering a compact packing arrangement of spherical nanoparticles: [Pd_{1678}(**4**)$_{336}$]; **Pd5c**: Found: C, 26.8; H, 2.4; N, 0.9; Pd, 57.3. Calc. for Pd_5(**5**)$_{0.6}(THF)_{1.2}$: C, 29.4; H, 3.0; N, 1.0; Pd, 62.1%; idealized formula taking into account the size determined by TEM and considering a compact packing arrangement of spherical nanoparticles: [Pd_{497}(**5**)$_{60}(THF)_{119}$]; **Pd6c**: Found: C, 29.6; H, 3.5; N, 1.4; Pd, 45.3. Calc. for Pd_5(**6**)$_{0.6}(THF)_4$: C, 34.7; H, 4.7; N, 1.7; Pd, 52.6%; idealized formula taking into account the size determined by TEM and considering a compact packing arrangement of spherical nanoparticles: [Pd_{288}(**6**)$_{35}(THF)_{230}$])

From decomposition of [Pd(ma)(nbd)]. 0.17 mmol of palladium precursor [Pd(ma)(nbd)] (50 mg) and 0.2 equivalents of ligand (0.034 mmol; 13.6 mg for **1**; 14.3 mg for **2**; 11.7 mg for **3**; 11.8 mg for **4**; 13.4 mg for **5**; 10.7 mg for **6**) were dissolved in 80 cm^3 of dried and degassed THF, and the system was then pressurised with three bar of hydrogen in a Fischer–Porter bottle. The reagents were dissolved in 80 cm^3 of dry THF and the system was pressurised with three bar of dihydrogen. In few minutes, the initially cream solution became grey. The reaction mixture was then stirred at room temperature for 18 h. The hydrogen was replaced by argon and the volatiles removed under reduced pressure. The resulting black solid was further washed with diethyl ether (3 × 5 cm^3), concentrated *in vacuum* and then dispersed in 2 cm^3 of THF for TEM analyses. The isolated particles were also analysed by IR spectroscopy and elemental analysis.

(**Pd3d**: Found: C, 18.7; H, 2.1; N, 0.6; Pd, 71.0. Calc. for Pd_5(**3**)$_{0.2}(THF)_{1.3}(H_2O)_{4.2}$: C, 15.0; H, 2.1; N, 0.7; Pd, 69.1%; **Pd4d**: Found: C, 18.3; H, 1.6; N, 0.7; Pd, 65.4. Calc. for Pd_5(**4**)$_{0.4}(THF)_{0.6}(H_2O)_{5.7}$: C, 18.7; H, 0.7; N, 1.6; Pd, 65.0%; **Pd5d**: Found: C, 36.2; H, 2.9; N, 1.2; Pd, 40.3. Calc. for Pd_5(**5**)$(THF)_{2.5}(H_2O)_{9.5}$: C, 34.7; H, 5.2; N, 1.1; Pd, 41.6%; idealized formula taking into account the size determined by TEM and considering a compact packing arrangement of spherical nanoparticles: [Pd_{259}(**5**)$_{52}(THF)_{130}(H_2O)_{492}$]; **Pd6d**: Found: C, 12.3; H, 1.3; N, 0.6; Pd, 77.8. Calc. for Pd_5(**6**)$_{0.15}(THF)(H_2O)_2$): C, 12.7; H, 2.3; N, 0.6; Pd, 77.4%.

General procedure for catalytic Suzuki C–C coupling

The preformed nanoparticles prepared as described above (0.01 mmol, 1.0 mol%), phenyl boronic acid (183 mg, 1.5 mmol, 1.5 eq) and Na_2CO_3 (212 mg, 2.0 mmol, 2 eq) dissolved in 1.0 cm^3 of deoxygenated water were solubilised in 3 cm^3 of dried toluene. 1.0 mmol of substrate was then added (0.13 cm^3 for

Table 3 Crystal data for **C6·3H$_2$O**

	C6·3H$_2$O
Empirical formula	C26 H38 N2 O7 Pd
Formula weight	596.98
T/K	173(2)
Wavelenght/Å	0.71073
Crystal system	Monoclinic
Space group	$P2_1/c$
a/Å	11.2894(4)
b/Å	11.9637(5)
c/Å	20.1191(8)
α (°)	90
β (°)	101.045(2)
γ (°)	90
Volume/Å^3	2667.01(18)
Z	4
Dc/Mg m^{-3}	1.487
Absorption coefficient/mm^{-1}	0.742
F(000)	1240
Cyrstal size/mm	0.10 × 0.05 × 0.05
θ range for data collection/°	5.12 to 24.71
Index ranges	$-11 <= h <= 13$, $-13 <= k <= 13$, $-18 <= l <= 23$
Reflections collected	12249
Independent reflections [R_{int}]	4468 [0.0631]
Refinement method	Full-matrix least squares on F^2
Observed reflections [$I > 2\sigma(I)$]	
Data/Parameters [restraints]	4468/18 [347]
Goodness-of-fit on F^2	0.827
Final R indices [$I > 2\sigma(I)$]	$R_1 = 0.0371$, w$R_2 = 0.0547$
R indices (all data)	$R_1 = 0.0715$; w$R_2 = 0.0606$
Largest diff. peak/hole/e Å^{-3}	0.461/−0.411

4-bromoanisole, 0.14 cm^3 for 4-bromobenzotrifluoride, 0.18 cm^3 for 4-bromodiphenylether, 0.20 cm^3 for 4-bromothioanisole). The resulting biphasic system was heated at 65 °C during 6 h and then cooled at room temperature. The organic phase (0.1 cm^3) was diluted in 2 cm^3 of diethyl ether and filtered on Celite. The mixture was consecutively washed with 2 cm^3 of 1 M NaOH and water, and the organic phase was dried on Na_2SO_4, filtered and analysed by gas chromatography to determine the substrate conversion.

Crystal structure determination

Yellow crystals of **C6·3H$_2$O** obtained from a dichloromethane/ether dissolution of the complex were selected and mounted on a Bruker-AXS APEXII diffractometer with graphite-monochromatized Mo-Kα radiation (λ = 0.71073 Å) at 173 K. Crystal data are summarized in Table 3. The structure was solved by direct methods[22] and all non hydrogen atoms were refined anisotropically using the least-squares method on F^2.[23] CCDC 770513 contains the supplementary crystallographic data for this paper.† These data can be obtained free of charge *via* www.ccdc.cam.ac.uk/conts/retrieving.htcm-3 (or from the CCDC, 12 Union Road, Cambridge CB2 1EZ, UK; fax: +44 1223 336033; e-mail: deposit@ccdc.cam.ac.uk).

Acknowledgements

The authors thank C. Pradel for his helpful contribution concerning TEM analyses, and the Centre National de la Recherche Scientifique (CNRS) and the Université Paul Sabatier for financial support. D. S. is grateful to the Ministère de l'Enseignement Supérieur et de la Recherche for a PhD research grant.

Notes and references

1 J. Tsuji, in *Palladium reagents and catalysts*, John Wiley & Sons, Sussex, United Kingdom, 2004.
2 For selected recent reviews, see: L. Duran Pachón and G. Rothenberg, *Appl. Organomet. Chem.*, 2008, **22**, 288–299; D. Astruc, *Angew. Chem. Int. Ed.*, 2005, **44**, 7852–7872; B. Chaudret, *Top. Organomet. Chem.*, 2005, **16**, 233–259; M. Moreno-Mañas and R. Pleixats, *Acc. Chem. Res.*, 2003, **36**, 638–643; A. Roucoux, J. Schultz and H. Patin, *Chem. Rev.*, 2002, **101**, 3757–3778; H. Bönnemann and R. M. Richards, *Eur. J. Inorg. Chem.*, 2001, 2455–2480; J. A. Widegren and R. G. Finke, *J. Mol. Catal. A: Chem.*, 2003, **198**, 317–341.
3 J. Durand, E. Teuma and M. Gómez, *Eur. J. Inorg. Chem.*, 2008, 3577–3586 references therein.
4 S. Jansat, J. Durand, I. Favier, F. Malbosc, C. Pradel, E. Teuma and M. Gómez, *ChemCatChem*, 2009, **1**, 244–246.
5 M. Tamura and H. Fujihara, *J. Am. Chem. Soc.*, 2004, **125**, 15742–15743; S. Jansat, M. Gómez, K. Philippot, G. Muller, E. Guiu, C. Claver, S. Castillón and B. Chaudret, *J. Am. Chem. Soc.*, 2004, **126**, 1592–1593; I. Favier, M. Gómez, G. Muller, M. R. Axet, S. Castillón, C. Claver, S. Jansat, B. Chaudret and K. Philippot, *Adv. Synth. Catal.*, 2007, **349**, 2459–2469.
6 I. Favier, S. Massou, E. Teuma, K. Philippot, B. Chaudret and M. Gómez, *Chem. Commun.*, 2008, 3296–3298.
7 J. A. Seetula, *J. Mol. Catal. A: Chemical*, 2005, **231**, 153–159; A. Bisi, S. Gobbi, A. Rampa, F. Belluti, L. Piazzi, P. Valenti, N. Gyemant and J. Molnar, *J. Med. Chem.*, 2006, **49**, 3049–3051.
8 W. K. Anderson and A. S. Milowsky, *J. Org. Chem.*, 1985, **50**, 5423–5424.
9 A. Sanyal, Q. Yuan and J. K. Snyder, *Tetrahedron Lett.*, 2005, **46**, 2475–2478; K. L. Burgess, N. J. Lajkiewicz, A. Sanyal, W. Yan and J. K. Snyder, *Org. Lett.*, 2005, **7**, 31–34.
10 A. Sasaoka, Md. I. Uddin, A. Shimomoto, Y. Ichikawa, M. Shiro and H. Kotsuki, *Tetrahedron: Asymmetry*, 2006, **17**, 2963–2969.
11 Y. Okuyama, H. Nakano, M. Igarashi, C. Kabuto and H. Hongo, *Heterocycles*, 2003, **59**, 635–643.
12 D. Sanhes, I. Favier, N. Saffon, E. Teuma and M. Gómez, *Tetrahedron Lett.*, 2008, **49**, 6720–6723.
13 D. Sanhes, A. Gual, S. Castillón, C. Claver, M. Gómez and E. Teuma, *Tetrahedron: Asymmetry*, 2009, **20**, 1009–1014.
14 A search on Cambridge Structural Database (CSD, Version 5.31 updates February 2010) reveals 30 related structures for imide derivatives containing 9,10-dihydroanthracene backbone, some of them crystallized with different solvent molecules.
15 We previously reported palladium and rhodium complexes containing diphosphite ligands where the phosphorous moieties are bonded to a 9,10-dihydroanthracene backbone, but we could not crystallize them (ref. 13).
16 K. Philippot and B. Chaudret, *C. R. Chimie*, 2003, **6**, 1019–1034.
17 K. Itoh, F. Ueda, K. Hirai and Y. Ishii, *Chem. Lett.*, 1977, **6**, 877–880.
18 J. Turkevitch, *Gold Bull.*, 1985, **18**, 125–131; M. A. Watzky and R. G. Finke, *J. Am. Chem. Soc.*, 1997, **119**, 10382–10400; A. Watzky and R. G. Finke, *Chem. Mater.*, 1997, **9**, 3083–3095; M. A. Watzky, E. E. Finney and R. G. Finke, *J. Am. Chem. Soc.*, 2008, **130**, 11959–11969.
19 Y.-C. Lai, H.-Y. Chen, W.-C. Hung, C.-C. Lin and F.-E. Hong, *Tetrahedron*, 2005, **61**, 9484–9489.
20 A. Jutand and A. Mosleh, *Organometallics*, 1995, **14**, 1810–1817.
21 C. C. Cassol, A. P. Umpierre, G. Machado, S. I. Wolke and J. Dupont, *J. Am. Chem. Soc.*, 2005, **127**, 3298–3299; J. G. de Vries, *Dalton Trans.*, 2006, 421–429; F. Fernández, B. Cordero, J. Durand, G. Muller, F. Malbosc, Y. Kihn, E. Teuma and M. Gómez, *Dalton Trans.*, 2007, 5572–5581.
22 *SHELXS-97*, G. M. Sheldrick, *Acta Crystallogr.* 1990, *A46*, 467-473.
23 *SHELXL-97*, Program for Crystal Structure Refinement, G. M. Sheldrick, University of Göttingen 1997.

